Materials Letters 190 (2017) 52–55

Contents lists available at ScienceDirect

Materials Letters

journal homepage: www.elsevier.com/locate/mlblue

Enhanced sodium ion batteries performance by the phase transition from hierarchical Fe_2O_3 to Fe_3O_4 hollow nanostructures

Kaiqiang Zhou [a,b], Yichao Zhen [a], Zhensheng Hong [a,b,*], Juhua Guo [c], Zhigao Huang [a,b]

[a] College of Physics and Energy, Fujian Normal University, Fujian Provincial Key Laboratory of Quantum Manipulation and New Energy Materials, Fuzhou 350117, China
[b] Fujian Provincial Collaborative Innovation Center for Optoelectronic Semiconductors and Efficient Devices, Xiamen 361005, China
[c] College of Chemistry and Chemical Engineering, Fujian Normal University, Fuzhou, Fujian 350007, China

ARTICLE INFO

Article history:
Received 17 September 2016
Received in revised form 16 December 2016
Accepted 18 December 2016
Available online 22 December 2016

Keywords:
Energy storage and conversion
Nanocrystalline materials
Sodium ion batteries

ABSTRACT

Hierarchical Fe_3O_4 hollow nanostructures are synthesized from the phase transition of Fe_2O_3 hollow nanostructures, which are prepared through a dissolution-recrystallization process. The hierarchical Fe_3O_4 hollow nanostructures, applied as an anode material for Na-ion batteries, display good rate capability and cycling stability. The reversible capacity of 150 mAh/g at 100 mA/g after 50 cycles can be maintained for Fe_3O_4 anode. The superior Na-ion storage properties of hierarchical Fe_3O_4 could be largely ascribed to the stable electrode structure during Na-ion insertion and extraction process. On the contrary, Fe_2O_3 anode exhibits a high initial discharge capacity (686 mAh/g), but it suffers from poor cycling stability due to the remarkable pulverization of the electrode.

1. Introduction

In recent years, sodium ion batteries (SIBs) have recently attracted lots of attentions due to the material abundance and low cost [1,2]. Now, a major obstacle in realizing SIBs is the absence of efficient anode materials [3]. Hence, developing suitable anode materials is a significant work for enhancing the performance of SIBs [4]. Because of the high theoretical capacity, transition metal oxides have been used as the electrochemical energy storage materials for SIBs [5]. In the past few years, some conversion reaction (Co_3O_4, MoS_2, $NiCo_2O_4$ and Fe_2O_3) anode materials were successfully applied as anode materials for SIBs by many groups [6–10]. Among them, Fe-basis materials are considered as promising anode materials owing to its high abundance and non-toxicity [9]. The major weakness of the Fe-basis materials is the large volume change during cycling, resulting in poor cycling stability [10].

In this work, the hierarchical Fe_3O_4 hollow nanostructures were synthesized by the phase transition of Fe_2O_3 hollow nanostructures, which were fabricated through a dissolution-recrystallization process of metal-organic complexes precursors. Moreover, hierarchical Fe_3O_4 hollow nanostructures demonstrate much better rate capability and cycling stability compared with Fe_2O_3 for Na-ion storage.

2. Experimental

For the synthesis of hierarchical hollow Fe_2O_3, 181 mg $FeCl_3{\cdot}6H_2O$, 166 mg 1, 4-benzenedicarboxylic acid (H_2bdc) and 10 mL N,N-dimethylformamide (DMF) was added into a 25 mL Teflon-lined under stirring, and then 2 mL 0.2 M NaOH was added into the solution and stirred for 10 min. Subsequently, the Teflon-lined was put into autoclave and heated at 150 °C from 45 min to 6 h. The products were obtained by centrifugation, washed with distilled water and ethanol several times and dried at 60 °C for 12 h. Finally, the products were annealed at 300 °C and 400 °C under Ar atmosphere to obtain Fe_2O_3 and Fe_3O_4 samples, respectively.

The active materials were admixed with super-P (SCM Industrial Chemical Co. Ltd.) and polyvinylidene fluoride (PVDF, SCM) binder additive in a weight ratio of 70:15:15. The mixture was pressed on circular copper foils as working electrodes (WE), and dried at 120 °C in vacuum for 12 h. Sodium-ion cells were assembled in coin-type cells (CR 2025) with a sodium metal foil (Aladdin) as the negative electrode, glass fiber separator (Whatman GF/F), and 1 M $NaClO_4$ in EC and diethyl carbonate (DEC) (1/1 in volume) as the electrolyte. Cyclic voltammetry (CV) measurements were performed on Zennium (Zahner).

* Corresponding author at: College of Physics and Energy, Fujian Normal University, Fujian Provincial Key Laboratory of Quantum Manipulation and New Energy Materials, Fuzhou 350117, China.
E-mail address: winter0514@163.com (Z. Hong).

http://dx.doi.org/10.1016/j.matlet.2016.12.055
0167-577X/

3. Results and discussion

Fig. 1a shows the X-ray diffraction (XRD) patterns of the fresh Fe_2O_3 and the samples obtained at different temperature. The sample harvested from a one-step solvothermal method for 3 h is pure Fe_2O_3 (JCPDS No.33-0664) based on the XRD results. The phase of Fe_2O_3 can be maintained at 300 °C with the Ar flow, but it would be entirely translated to pure Fe_3O_4 (JCPDS No. 65-3107) after heat treatment at 400 °C for 2 h. Similar phenomenon was also found in the previous report [11]. The reaction equation is as follows:

$$6Fe_2O_3 + C \rightarrow Fe_3O_4 + CO_2$$

Meanwhile, the average crystallite size of the Fe_3O_4 and Fe_2O_3 particle is calculated to be about 18 nm and 15 nm using the Scherer equation, based on the most intensive diffraction peak. Thermogravimetric analysis (TGA) reveals that the content of the carbon is about 3.7% in the as-prepared Fe_3O_4 and 6.8% in the Fe_2O_3, shown in the Fig. S1.

The morphology and structure of the as-prepared samples were characterized by scanning electron microscopy (SEM) and transmission electron microscopy (TEM). As shown in the Fig. S2, the as-prepared Fe_2O_3 particles (about 80–100 nm) basically have similar morphology and size with Fe_3O_4. From the high-magnification SEM images (Fig. 1b and c), it could be observed that both Fe_2O_3 and Fe_3O_4 were constructed by small nanoparticle subunits. The TEM images (the inset in Fig. 1b and c) further confirm the hierarchical hollow morphology of Fe_2O_3 and Fe_3O_4. Fig. 1d shows the HRTEM image of Fe_3O_4 nanostructures, the clear lattice fringes of ca. 0.26 nm can be assigned to the spacing of (311). Besides, the Fe_3O_4 nanocrystals were coated with a thin carbon layer (about 1–2 nm).

In order to reveal the synthetic process, the Fourier Transform Infrared Spectrometer (FT-IR) was used to analyze the samples obtained at different reaction conditions and the results are depicted in Fig. S3. It demonstrates that the product fabricated at 150 °C for 45 min is the metal-organic coordination complexes. Fig. 2 shows the SEM images of the products obtained at different reaction times under solvothermal condition. A lot of nanorods precursors harvested from 45 min reaction are observed from Fig. 2a. When the reaction times increased to 2 h, most nanorods disappear or dissolve and many particles with square shape appear, as shows in Fig. 2b. Pure square particles were fabricated after 6 h (Fig. 2d). According to the above results, it's suggested that hierarchical Fe_2O_3 hollow nanostructures were synthesized by a dissolution-recrystallization process.

In order to investigate the electrochemical performance of the Fe_3O_4, the cyclic voltammetry (CV) was tested at a scan rate of 0.5 mV/s in the voltage range of 0.01–3 V. From Fig. 3a, a cathodic peak around 0.5 V is observed which corresponds to the conversion reactions of Fe^{2+}/Fe^{3+} to their metallic states and the formation of Na_2O. The broad anodic peak around 1.5 V is ascribed to the oxidation reactions of metallic Fe [12,13]. The conversion reaction of Fe-based oxides as follows [11,12]:

$$Fe_2O_3 + 6Na^+ + 6e^- \leftrightarrow 2Fe + 3Na_2O$$

$$Fe_3O_4 + 8Na^+ + 6e^- \leftrightarrow 3Fe + 4Na_2O$$

Fig. 3b exhibits the charge-discharge profiles of the Fe_3O_4 electrode at 50 mA/g. The initial discharge and charge capacity of 442 mAh/g and 220 mAh/g are obtained, respectively. The larger irreversible reaction at the first cycle for the electrode material and solid electrolyte interface (SEI) formed on the surface of the electrode [9–10]. As shown in Fig. 3c, Fe_3O_4 anode maintained a stable capacity of 80 mAh/g at a high current of 1000 mAh/g, demonstrating a good rate capability.

The cycling performance of the Fe_3O_4 and Fe_2O_3 at a constant current density of 100 mA/g is presented in Fig. 3d. Fe_2O_3 displays a larger initial discharge capacity (686 mAh/g) compared with Fe_3O_4 (392 mAh/g) at the first cycle, which could be due to its high valence state of iron element. However, it is noted that the cycling

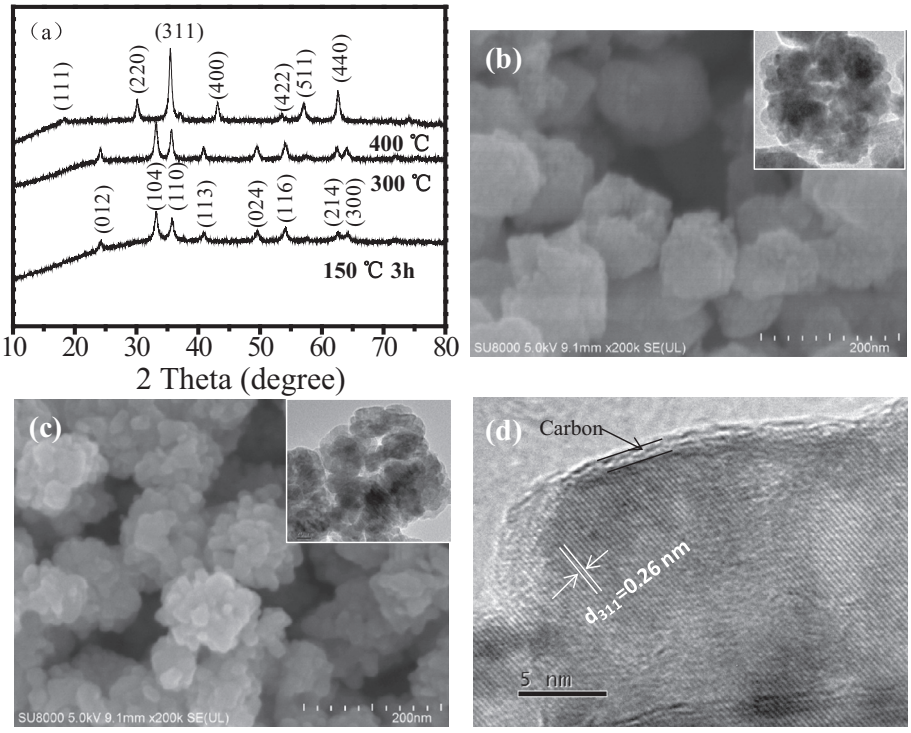

Fig. 1. (a) XRD patterns of the fresh Fe_2O_3 and the samples annealed at different temperatures, SEM images of (b) Fe_2O_3 and (c) Fe_3O_4 obtained at 300 and 400 °C, (d) HRTEM image of Fe_3O_4. The insets in (b) and (c) are the TEM image of Fe_2O_3 and Fe_3O_4.

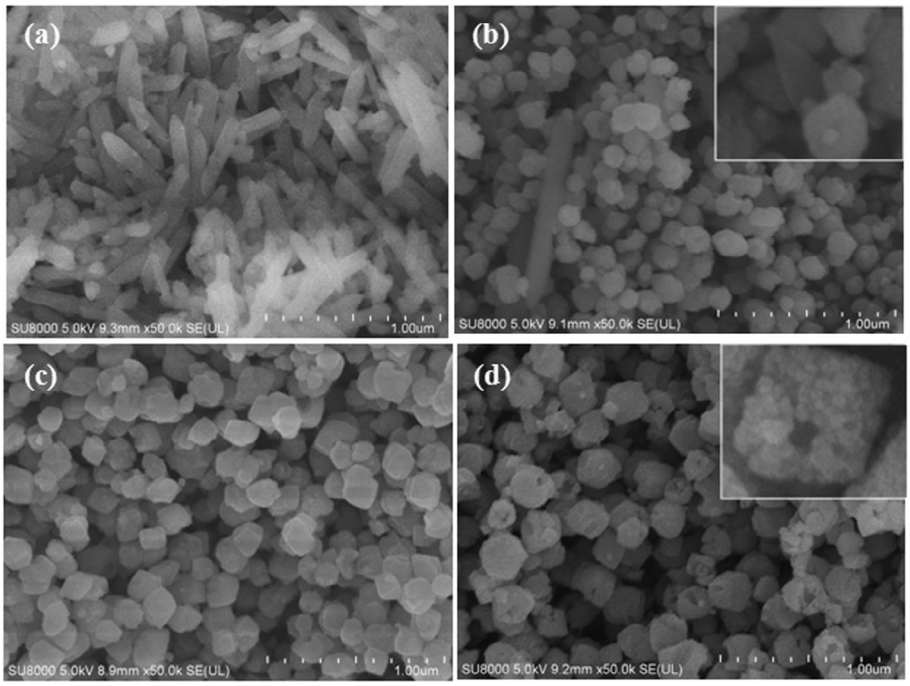

Fig. 2. SEM images of the products obtained at different reaction times under solvothermal condition: (a) 45 min, (b) 2 h, (c) 3 h and (d) 6 h. The insets in (b) and (d) are the enlarged SEM images.

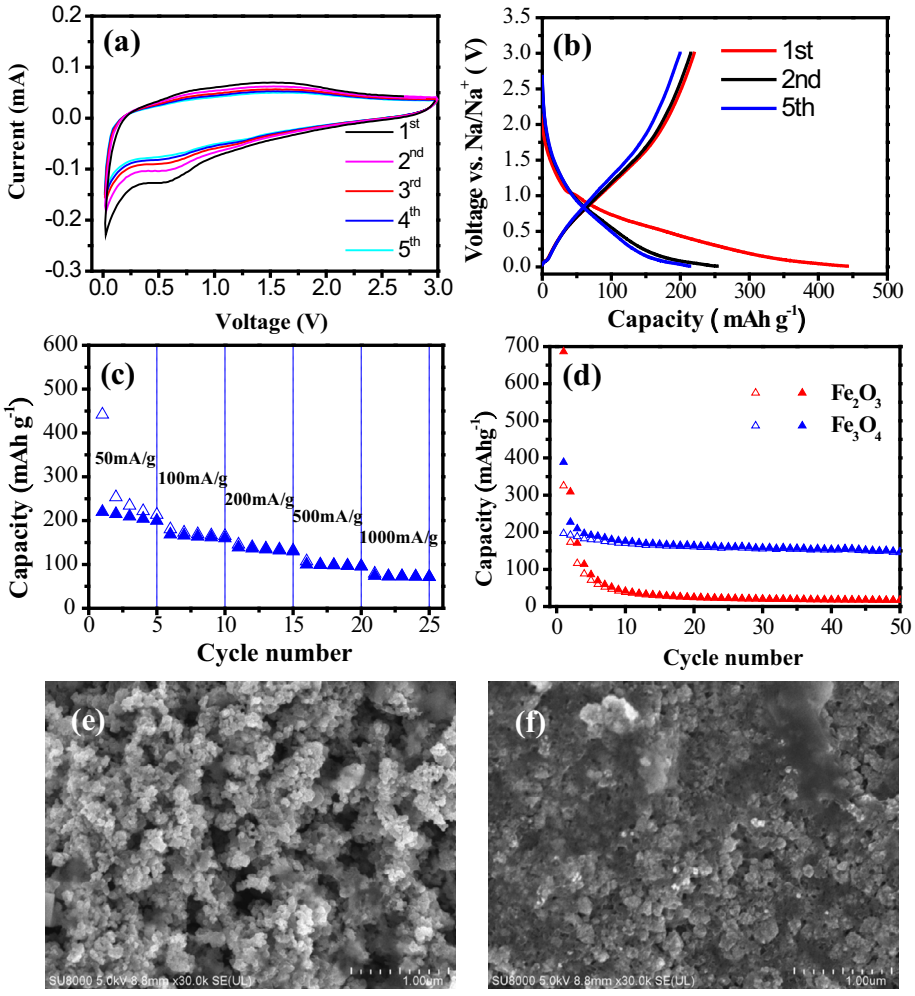

Fig. 3. (a) CV curves of the Fe_3O_4 at a scan rate of 0.5 mV/s, (b) galvanostatic discharge and charge profiles of Fe_3O_4 at the selective cycles, (c) rate capability for Fe_3O_4 at the current densities from 50 to 1000 mA/g, (d) cycling performance of Fe_2O_3 and Fe_3O_4 at a current density of 100 mA/g, SEM images of Fe_2O_3 (e) and Fe_3O_4 (f) electrodes after cycling test.

stability of the Fe_2O_3 is poor, a capacity less than 12 mAh/g were remained after 20 cycles. On the contrary, a capacity of 150 mAh/g can be retained for Fe_3O_4 even after 50 cycles. In order to open out this difference, the morphology of the electrodes of Fe_2O_3 and Fe_3O_4 after 50 cycles were characterized by SEM images, as depicted in Fig. 3e-f. A large number of cavities in the electrode of Fe_2O_3 can be clearly observed from the Fig. 3e and many of the hierarchical hollow nanostructures were broken. This could be ascribed to the collapse or pulverization phenomenon of the electrode because of the large volume change. Contrarily, the well compact structure and morphology of Fe_3O_4 electrode can be maintained after cycling test (Fig. 3f). Although Fe_2O_3 and Fe_3O_4 have a similar electrochemical reaction, the higher valence state of Fe in Fe_2O_3 suffered from larger volume change, which may be the main reason for their different Na-ion storage performance. This suggests that Fe_3O_4 can effectively accommodate the volume change during Na^+ insertion and extraction process and alleviate the pulverization, leading to good cycling stability.

4. Conclusion

In summary, hierarchical Fe_3O_4 hollow nanostructures have been prepared from the phase transition of Fe_2O_3 hollow nanostructures. When the Fe_3O_4 and Fe_2O_3 hollow nanostructures were studied as anode materials for SIBs, Fe_3O_4 exhibits much better performance, including superior rate capability and good cycling stability. The poor cycling stability of Fe_2O_3 could be due to the collapse or pulverization of the electrode because of the large volume change. However, it's notable that Fe_3O_4 can effectively accommodate the volume change during Na^+ insertion and extraction process and alleviate the pulverization, leading to good cycling stability. This result provides a good insight of the Fe-based oxides electrode material for rechargeable batteries.

Acknowledgements

This work was financially supported by National Natural Science Foundation of China (NSFC 51502038, 21406035), National Science Foundation of Fujian Province (2015J01042), and Education Department of Fujian Province (JA14081 and JA14076).

Appendix A. Supplementary data

Supplementary data associated with this article can be found, in the online version, at http://dx.doi.org/10.1016/j.matlet.2016.12.055.

References

[1] Y.F. Zhang, L.Q. Li, H.Q. Su, W. Huang, X.C. Dong, J. Mater. Chem. A 3 (2015) 43.
[2] N. Yabuuchi, K. Kubota, M. Dahbi, S. Komaba, Chem. Rev. 114 (2014) 11636–11682.
[3] Z.S. Hong, K.Q. Zhou, Z.G. Huang, M.D. Wei, Sci. Res. 5 (2015) 11960.
[4] D. Chen, Q.F. Wang, R.M. Wang, G.Z. Shen, J. Mater. Chem. A3 (2015) 10158.
[5] Y. Kim, K.H. Ha, S.M. Oh, K.T. Lee, Chem. Eur. J. 20 (2014) 11980–11992.
[6] Z.L. Jian, P. Liu, F.J. Li, M.W. Chen, H.S. Zhou, J. Mater. Chem. A 2 (2014) 13805.
[7] Z. Hu, L. Wang, K. Zhang, J. Wang, F. Cheng, Z. Tao, J. Chen, Angew. Chem. Int. Ed. 53 (2014) 12794–12798.
[8] K.Q. Zhou, Z.S. Hong, C.B. Xie, H. Dai, Z.G. Huang, J. Alloys Comp. 651 (2015) 24–28.
[9] S.H. Lee, S.H. Yu, J.E. Lee, A. Jin, D.J. Lee, N. Lee, H. Jo, K. Shin, T.Y. Ahn, Y.-W. Kim, Nano Lett. 13 (2013) 4249–4256.
[10] T. Muraliganth, A.V. Murugan, A. Manthiram, Chem. Commun. 47 (2009) 7360–7362.
[11] B. David, O. Schneeweiss, N. Pizúrová, F. Dumitrache, C. Fleaca, R. Alexandrescu, Surf. Interface Anal. 42 (2010) 699–702.
[12] D. Li, S. Wu, F. Wang, S. Jia, Y. Liu, X. Han, L. Zhang, S. Zhang, Y. Wu, Mater. Lett. 178 (2016) 48–51.
[13] X. Meng, Y. Xu, X. Sun, J. Wang, L. Xiong, X. Du, S. Mao, J. Mater. Chem. A 3 (2015) 12938–12946.